Chapter 9

Analysis of Biomass Waste Cofiring into Existing Coal-Fired Power Plant Using Computational Fluid Dynamics

Arif Darmawan, Dwika Budianto,
Koji Tokimatsu and Muhammad Aziz

Additional information is available at the end of the chapter

http://dx.doi.org/10.5772/intechopen.70561

Abstract

Biomass utilization to generate electricity via combustion simply can be classified into firing and cofiring. Biomass cofiring into the pulverized coal boilers has some advantages compared to dedicated biomass firing in terms of capital cost and combustion efficiency. To understand the cofiring behavior of biomass and coal comprehensively, computational fluid dynamics (CFD) method can be used to analyze and solve problems involving fluid flows inside a combustor. A CFD modeling is significantly more effective from the perspectives of time and cost and safety and ease of scaling up; hence, it is usually performed before conducting a physical investigation through experiment. Moreover, the current state-of-the-art CFD modeling-based study is capable of solving the complexity of the interdependent processes such as turbulence, heat transfer via radiation, produced gas, and reactions in both the particle and gas phases during combustion. This chapter focuses on the study of cofiring of biomass, which is palm mill wastes, into the existing coal-fired power plant. Two palm mill wastes are evaluated: palm kernel shell and hydrothermally treated empty fruit bunch. Distributions of temperature and the produced are simulated to find the most optimum and applicable cofiring conditions.

Keywords: cofiring, computational fluid dynamics, modeling, waste biomass, coal, temperature distribution

1. Introduction

Biomass utilization through cofiring into existing coal-fired power plants or ones being constructed/planned becomes very important. Several European countries, Japan, and several coal-dependent countries such as China have implemented cofiring technology in their newly built coal-fired power plant with the biomass having a blending percentage of 10–20% in

calorie basis [1]. Biomass cofiring with coal is believed to be able to enhance the domestic energy security through renewable energy utilization as well as improve the utilization of power plants that were initially designed for coal. To understand the cofiring behavior of biomass and coal inside the combustor, numerical method of computational fluid dynamics (CFD) can be used to analyze and solve problems involving fluid flows. This method is usually adopted before performing an experimental investigation.

To understand this issue comprehensively, this chapter is divided into three main parts:

- Scheme and technical aspects of biomass cofiring with coal
- Modeling approach to predict combustion behavior of cofiring biomass waste in existing coal-fired power plant
- Case study of palm oil waste cofiring (including result and discussion).

In Section 2, a brief knowledge about the technical aspects of biomass cofiring with coal is presented. In the next part (Section 3), CFD modeling for biomass cofiring with coal is reported. Furthermore, in Section 4, a case study of palm oil waste cofiring with coal will be discussed to evaluate the applicability of the CFD models. The palm oil waste reported in the Section 4 consists of palm kernel shell (PKS) and hydrothermally treated empty fruit bunch (HT-EFB) [2, 3].

Employing CFD to assist the cofiring behavior can give a deep discussion and a scientific knowledge to the reader. Scientists, engineers, and others who are interested in learning CFD and its current developments in biomass conversion technologies will find this chapter invaluable. Moreover, by understanding the CFD method, hopefully it can further be replicated into different biomass feedstocks and scales, depending on the research goal.

2. Retrofitting the existing coal power plants through cofiring for sustainable energy

In the future, biomass will play a significant role in many countries as energy source. The utilization of biomass using an appropriate technology is important to optimize its economic benefit and minimize the environmental impacts. The appropriate technology means applicable in small- and large-scales, energy-efficient, environmentally friendly, and decentralized. Some conversion techniques have been studied and applied in the recent years from small laboratory-scale up to large-scale, such as: pyrolysis, direct-combustion, gasification, and anaerobic digestion. In thermal conversion, direct-combustion is generally performed in the boilers or furnaces to produce steam that can be used for district heating or driving the turbines in power generation.

Utilization of biomass to generate electricity via direct-combustion can be technically classified into two types: firing and cofiring. Biomass cofiring to the existing power plants (as

http://dx.doi.org/10.5772/intechopen.70561

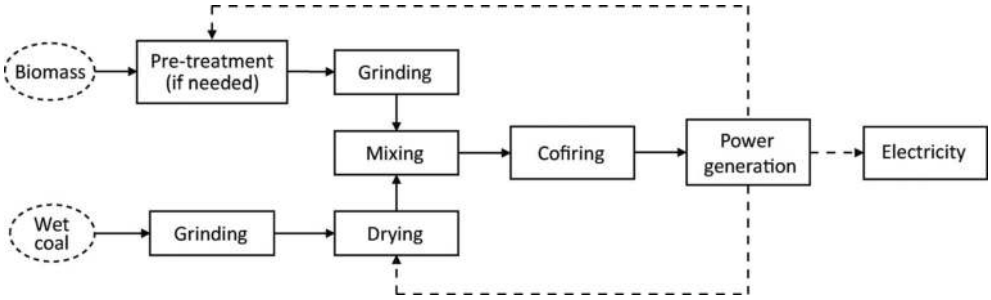

Figure 1. Basic schematic diagram of biomass and coal cofiring system.

shown in **Figure 1**), especially coal-fired power plants, has some advantages compared to dedicated biomass firing such as minimum capital cost and optimum combustion efficiency [2]. Other advantages of biomass cofiring into existing coal-fired power plant are that it can significantly reduce the emissions from the power plant and minimize the slagging inside combustor [3].

Biomass cofiring into coal-fired boilers can be performed in some different methods such as parallel cofiring, injection, pregasification, and comilling. Due to lower capital cost and high cofiring ratio, injection cofiring is the most feasible method applied in the industrial scale [4]. In this method, premilled biomass and pulverized coal are continuously mixed and cofed into the boiler.

Since developing countries are likely to put their future in the coal resources [5, 6], biomass cofiring seems to be a promising option for improving the energy sustainability and reducing the environmental impacts. Biomass can be classified into two categories: biomass waste and energy crops. In addition, properties such as moisture, nitrogen content are depending on their pretreatment [7]. For further discussion, it is also important to consider the biomass availability from the surrounding to avoid potential conflict, for example, with food production.

3. CFD modeling for coal and biomass cofiring inside a combustor

Once the fuel or mixed fuel is fed to the combustor, the following reactions occur continuously: preheating, evaporation or drying, devolatilization, gas-char combustion, pollutant generation, and radiation [8]. To understand this complex phenomenon, CFD is a powerful tool that can model and calculate fluid flows, heat and mass transfers, and chemical reactions as well as interactions of solids and fluids [9].

The general process for CFD-based combustion modeling is shown in **Figure 2**. CFD modeling method for the combustion of mixed biomass and coal particles is arguably a challenging

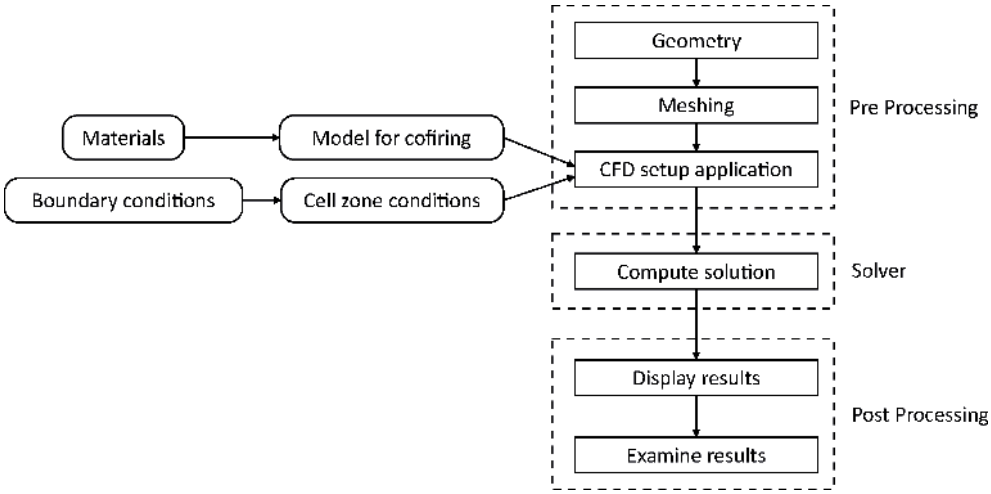

Figure 2. Summary of CFD process modeling.

work. However, compared to physical investigation through experiment, CFD modeling is considered more effective from both time and cost perspectives, as well as higher safety and easier scaling up. Hence, it is usually adopted before performing an experimental study. Related to cofiring using CFD analysis, it is expected that the combustion performance for all stages of the combustion including the combustion temperature, kinetic behavior, and concentration of the produced gases can be clarified. Cofiring simulation considers dynamical equations, conservation of mass (continuity), momentum and enthalpy, turbulence, radiation heat transfer, and reactions in both particle and gas phases [10].

3.1. Conservation equations

In the biomass cofiring, since combustion involves chemical reactions between mixed biomass-coal and an oxidant, the process is usually assumed and modeled as solid and gas or dilute two-phase flow which is approximated as Eulerian-Lagrangian equation. In this approach, the gas phase is modeled using Reynolds Averaged Navier-Stokes Equations (RANS) model. On the other hand, the solid phase is treated as a discrete phase. In addition, the trajectory of each particles is calculated using Newton's laws of motion in which the particles collision is considered using the sphere model [11]. Furthermore, both gas concentration and temperature distribution are approximated using the energy and mass transfer equations for the particles. The interactions of mass, momentum, and energy between the gas and solid particles are calculated using the particle-in-cell (PIC) approach with the consideration of particle state along the particle trajectories. The mathematical calculations are basically governed by the flow of fluid. In the conserved form, the continuity, momentum, and total energy conservations can be represented as Eqs. (1)–(5), respectively [12]:

$$\frac{\partial \rho}{\partial t} + \nabla \cdot \left(\rho \vec{V} \right) = 0 \tag{1}$$

$$\frac{\partial (\rho u)}{\partial t} + \nabla \cdot \left(\rho u \vec{V} \right) = -\frac{\partial p}{\partial x} + \frac{\partial \tau_{xx}}{\partial x} + \frac{\partial \tau_{yx}}{\partial y} + \frac{\partial \tau_{zx}}{\partial z} + \rho f_x \tag{2}$$

$$\frac{\partial (\rho v)}{\partial t} + \nabla \cdot \left(\rho v \vec{V} \right) = -\frac{\partial p}{\partial y} + \frac{\partial \tau_{xy}}{\partial x} + \frac{\partial \tau_{yy}}{\partial y} + \frac{\partial \tau_{zy}}{\partial z} + \rho f_y \tag{3}$$

$$\frac{\partial (\rho w)}{\partial t} + \nabla \cdot \left(\rho w \vec{V} \right) = -\frac{\partial p}{\partial z} + \frac{\partial \tau_{xz}}{\partial x} + \frac{\partial \tau_{yz}}{\partial y} + \frac{\partial \tau_{zz}}{\partial z} + \rho f_z \tag{4}$$

$$\frac{\partial}{\partial t}\left[\rho\left(e + \frac{V^2}{2}\right)\right] + \nabla \cdot \left[\rho\left(e + \frac{V^2}{2}\vec{V}\right)\right] = \rho \dot{q} + \frac{\partial}{\partial x}\left(k\frac{\partial T}{\partial x}\right) + \frac{\partial}{\partial y}\left(k\frac{\partial T}{\partial y}\right)$$

$$+ \frac{\partial}{\partial z}\left(k\frac{\partial T}{\partial z}\right) - \frac{\partial (up)}{\partial x} - \frac{\partial (vp)}{\partial y} - \frac{\partial (wp)}{\partial z} + \frac{\partial (u\tau_{xx})}{\partial x} + \frac{\partial (u\tau_{yx})}{\partial y} + \frac{\partial (u\tau_{zx})}{\partial z} + \frac{\partial (v\tau_{xy})}{\partial x} + \frac{\partial (v\tau_{yy})}{\partial y}$$

$$+ \frac{\partial (v\tau_{zy})}{\partial z} + \frac{\partial (w\tau_{xz})}{\partial x} + \frac{\partial (w\tau_{yz})}{\partial y} + \frac{\partial (w\tau_{zz})}{\partial z} + \rho \vec{f} \cdot \vec{V} \tag{5}$$

where, ρ, V, p, f, τ, k, and $\dot{q}$ are density, velocity, pressure, body force per unit mass, shear force, thermal conductivity, and heat transferred through thermal conduction per unit time per unit area, respectively. u, v, and w are velocity components in each x, y, and z directions, respectively. In addition, e, $V^2/2$, and $(e + V^2/2)$ are internal, kinetic energy per unit mass, and total energy, respectively. We can say, Eqs. (1)–(3) represent each of mass (continuity equation in nonconservation form, momentum, enthalpy energy) conservations, respectively. Moreover, Eqs. (4) and (5) relate to the calculation of temperature and specific mass fraction, correspondingly.

3.2. Behavior of turbulence flows during combustion

The flow in the combustor, usually called as "turbulence," is very important to be considered in the combustion simulation. This physical phenomenon influences both heat and mass transfers inside the combustor. Turbulence occurs due to the inertia of the fluid covering time-dependent and convective acceleration, and which is characterized by the velocity fluctuations because of the complex geometry and high flow rates. Due to good solution and effective time during computation, k-ε (k-epsilon) turbulence model is widely adopted to calculate the RANS equations that are employed to model the cofiring. In addition, in CFD modeling, this k-ε turbulence model is generally employed to determine and solve the swirling combustion flows. There are two main equations involved in this model relating to each turbulent kinetic energy, k, and turbulent dissipation rate, ε. Both of them can be expressed in the following Eqs. (6) and (7), respectively:

$$\frac{\partial}{\partial t}(\rho k) + \frac{\partial}{\partial x_i}(\rho k u_i) = \frac{\partial}{\partial x_j}\left[\frac{\mu_t}{\sigma_k}\frac{\partial k}{\partial x_j}\right] + 2\mu_t E_{ij}E_{ij} - \rho\epsilon \tag{6}$$

$$\frac{\partial}{\partial t}(\rho\epsilon) + \frac{\partial}{\partial x_i}(\rho\epsilon u_i) = \frac{\partial}{\partial x_j}\left[\left(\mu + \frac{\mu_t}{\sigma_\epsilon}\right)\frac{\partial \epsilon}{\partial x_j}\right] + C_{1\epsilon}\frac{\epsilon}{k}2\mu_t E_{ij}E_{ij} - \rho C_{2\epsilon}\frac{\epsilon^2}{k} \tag{7}$$

where, k, ϵ, u_i, and E_{ij} are turbulent kinetic energy, turbulent dissipation, velocity component in corresponding direction, and deformation rate component, respectively. Furthermore, the turbulent viscosity, μ_t, is calculated using Eq. (8).

$$\mu_t = \rho C_\mu \frac{k^2}{\epsilon} \tag{8}$$

where $C_{1\epsilon}$, $C_{2\epsilon}$, C_μ, σ_k, and σ_ϵ are constants.

3.3. Development of radiation models for cofiring

Since the combustion temperature is relatively high, attention should be given for heat transfer through radiation. It controls both heat transfer and heat flux, especially during heating, drying, flame ignition, devolatilization, and char combustion. The suitable model for radiation can be selected from different radiation models such as:

- Discrete-ordinates model (DOM)
- P-1 model
- Discrete transfer radiation method (DTRM)

For certain cases, one radiation model may be more appropriate than another, depending on the boundaries and system conditions. Each model has advantages and limitations. P-1 model is widely used for specific application to pulverized coal-fired boilers. In addition, some researchers are also adopting P-1 radiation model for their research related to cofiring [2, 3, 13]. The DO model is more expensive but has an accurate process and is applicable for a large range of optic thickness. Furthermore, the DTRM model is suitable for a large range of optic thickness with less accuracy than DO model [14].

3.4. Particle phase reaction mechanisms

In cofiring process, we can consider the mixture of biomass waste and coal as a typical gas-solid flow with their chemical reactions. Furthermore, Eulerian-Lagrangian model can be adopted to figure the hydrodynamics of the mixture. Both particles are modeled separately as two discrete phase models. There are some reactions involved in the particle phase, especially the char combustion. It is assumed as char oxidation to produce CO that is released to the bulk gas in the combustor. It is important to note that, in general, char from biomass is more reactive and has higher heating rate than one from coal.

During devolatilization, the volatile matters exhausted from each biomass and coal are released to the bulk gas and then have reaction with O_2 (oxidation). The general reactions in

both particle and gas phases for coal cofiring with biomass waste can be shown in the following reactions:

i. Char of coal

$$C + 0.5O_2 \rightarrow CO \tag{9}$$

ii. Char of biomass

$$C + 0.5O_2 \rightarrow CO \tag{10}$$

iii. Volatile matter of coal

$$CH_{\alpha 1}O_{\alpha 2}N_{\alpha 3}S_{\alpha 4} + {}_{\gamma 1}O_2 \rightarrow CO + {}_{\gamma 2}H_2O + {}_{\gamma 3}O_2 + {}_{\gamma 4}N_2 \tag{11}$$

iv. Volatile matter of biomass waste

$$CH_{\alpha 5}O_{\alpha 6}N_{\alpha 7}S_{\alpha 8} + {}_{\gamma 5}O_2 \rightarrow CO + {}_{\gamma 6}H_2O + {}_{\gamma 7}O_2 + {}_{\gamma 8}N_2 \tag{12}$$

and

$$CO + 0.5\,O_2 \rightarrow CO_2 \tag{13}$$

Composition and enthalpy formation for both biomass waste and coal are determined based on both proximate and ultimate analyses of each material. Therefore, the variables α and γ in the above reactions can be derived by proximate and ultimate analyses from each cofired material.

4. Case studies of biomass waste cofiring

4.1. Numerical analysis of cofiring of PKS into pulverized coal-fired boiler

4.1.1. Boiler dimensions and calculation conditions

The first step in the cofiring evaluation through CFD is determining the combustor or boiler dimensions and its layout of the meshing. The detailed part of the boiler is shown in **Figure 3**, including the feeding inlets in cross section. The boiler shape of this simulation referred to an existing coal-fired power plant with capacity 300 MWe. This boiler had a height, width, and breadth of 45, 12, and 15 m, correspondingly. To perform the simulation, a commercial CFD software was prepared. ANSYS DesignModeler was used to build the combustor model in 3D, and Fluent ver. 16.2 (ANSYS Inc.) is used to analyze the cofiring behavior. The cofiring simulation took account of governing equations (for mass, momentum, enthalpy, temperature, and specific mass fraction), turbulence, radiative heat transfer, and reactions for both the particle and gas phases.

The used biomass sample was PKS, which is one of solid wastes in palm milling to produce palm oil. The solid wastes in palm milling include empty fruit bunch (EFB), fiber, and PKS with ratios of about 23, 12, and 5%, respectively [15, 16]. Fiber is usually combusted inside the

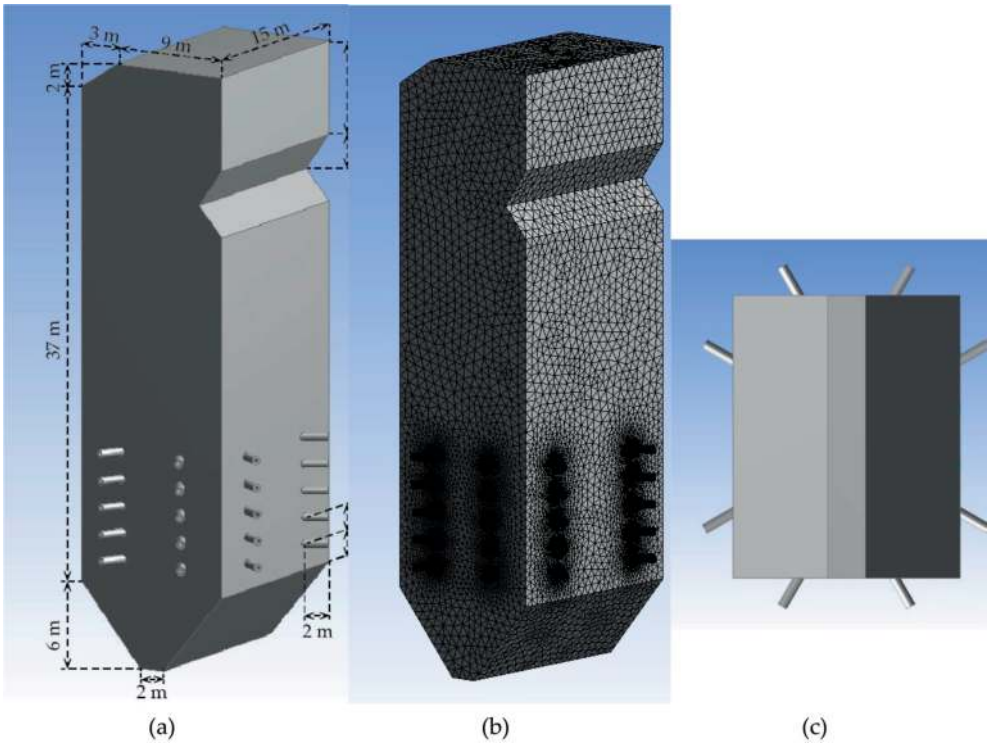

Figure 3. Schematic diagram of the boiler design: (a) boiler dimensions, (b) meshing layout, (c) inlet feed distribution (cross section).

mill to produce steam consumed for the milling, especially sterilization. In addition, an effective energy utilization of EFB has been proposed in previous studies [17, 18] for power generation. PKS has advantageous characteristics of low moisture content and higher calorific value, compared with those other solid wastes.

Both the coal and PKS characteristics are shown in **Table 1**. Since the case was designated to perform cofiring in Indonesia, the coal was collected from the country that is categorized as having low rank coal (LRC) with high moisture content. In addition, the PKS was obtained from a palm oil mill (POM) located in Sumatera Island. Due to high moisture content, initial drying was conducted in order to lower the moisture content up to 17.30%. Moreover, the PKS was used for cofiring with any initial pretreatment except grinding.

The fuel flow rates for coal and air under ambient condition were 73 and 630 kg s^{-1}, correspondingly. In addition, the air is approximated to contain N_2 and O_2 with concentrations of 79 mol% and 21 mol%, respectively. Each particle was regarded as to be a solid sphere, having particle sizes in the range of 60–200 mesh (74–250 μm). Furthermore, the bulk densities of the coal and PKS were considered to be 700 and 600 kg m^{-3}, respectively. The ambient temperature, combustor wall thickness, and external and internal emissivity coefficients were set at 300 K, 0.2 m, 0.9, and 0.6, respectively.

Component	Properties	Coal		PKS
		As-received	As-used	As-used
Proximate analysis (wt%)	Fixed carbon	24.93	40.23	24.35
	Volatile matter	25.76	41.57	66.77
	Moisture	48.76	17.30	3.86
	Ash	0.56	0.90	5.02
Ultimate analysis (wt%)	Carbon	35.30	56.98	43.77
	Hydrogen	2.29	3.69	5.85
	Oxygen	11.23	18.13	42.32
	Nitrogen	1.75	2.83	0.89
	Sulfur	0.11	0.17	0.00
LHV (MJ kg^{-1})		13.84	22.33	17.68

Table 1. Material composition of coal and PKS particles used in the study.

The simulation was performed using a Quad-core Intel Core i7 2.9 GHz CPU and 16 GB of RAM. The total mesh of the 3D model used to represent the combustor was an approximately 1,805,305 tetrahedral cell unstructured grid. In the CFD modeling, the temperature distribution and concentration of the produced gases (CO_2, CO, O_2, NO_x, and SO_x) were evaluated. In addition, five different PKS mass fractions were tested: 0% (100% coal), 10, 15, 25, and 50%.

4.1.2. Results and discussion

4.1.2.1. Temperature distribution

Temperature distribution for each PKS mass fraction is shown in **Figure 4**. Generally, higher PKS mass fraction leads to higher flame temperatures inside the boiler, since higher PKS mass fraction means larger amount of volatile matter emitted during cofiring. The average temperature in the upper part of boiler, especially at the freeboard, is lower than the lower part of boiler. It is considered as the result of heat loss across the boiler.

In **Table 1**, it can be observed that the used PKS has higher volatile matter and lower moisture content compared to the coal, since the used coal was LRC with relatively low calorific value. With this condition, the devolatilization of PKS particles would be faster and earlier than the devolatilization of the coal particles. It resulted in higher and more uniform combustion temperature at high PKS mass fraction. Because the water has a relatively high heat capacity, the increase of PKS mass fraction also leads to the decrease of the total moisture content of the mixed fuel, influencing the combustion temperature.

The average temperature at boiler outlet for PKS mass fractions of 0, 10, 15, 25, and 50% are 1390, 1414, 1422, 1513, and 1494 K, respectively. Although insignificant, cofiring with a PKS mass fraction of 25% resulted in higher combustion temperature compared to a mass fraction of 50%. In contrast to the moisture content, a higher PKS mass fraction decreased the total amount of fixed carbon (including char) in the mixed fuel. Therefore, the heat obtained from

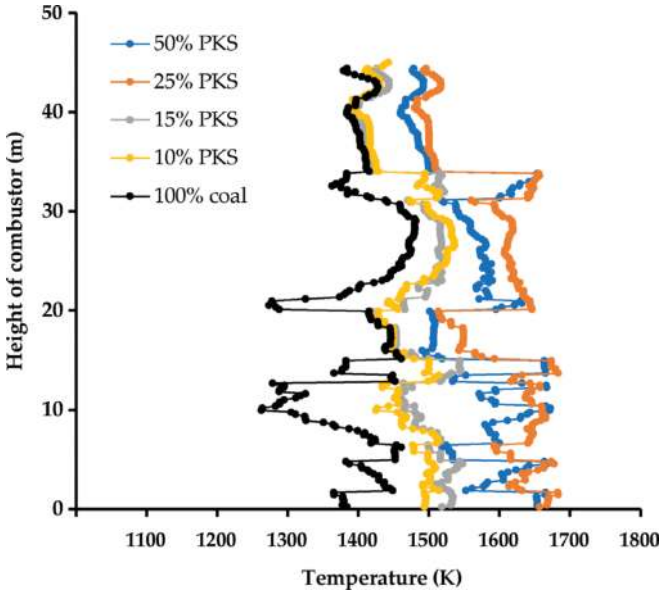

Figure 4. Temperature distribution at the center along the height of the boiler for each different PKS mass fraction.

the char combustion fell since the PKS mass fraction increased. The temperature distribution profile suggested that the optimum combustion performance of coal and PKS cofiring can be achieved at a PKS mass fraction of 25%.

4.1.2.2. Distribution of CO_2, CO, O_2, NO_x, and SO_x

Figures 5–7 [3] represent the CO_2, CO, and O_2 gases distribution inside the boiler, respectively. Generally, higher PKS mass fraction led to a lower CO_2 concentration, lower CO concentration, and higher CO_2, respectively. This is because PKS has a relatively high O_2 content, part of which persists and is exhausted together with the nitrogen and other flue gases.

Figures 8 and **9** [3] represent the cross-sectional NO_x and SO_x distribution at the center of the boiler. Higher PKS mass fraction leads to higher NO_x concentration and increased significantly as the PKS mass fraction increased to 25%. According to the Zeldovich mechanism [19], at above 1600 K, thermal NO_x generation can occur easily. The maximum combustion temperature at PKS mass fractions of 25 and 50% exceeded this value. This suggested that a lower PKS, of up to 15%, is the appropriate cofiring condition for limiting NO_x emissions.

4.2. Retrofitting existing coal power plants through cofiring with hydrothermally treated empty fruit bunch

4.2.1. Combustor dimensions and calculation conditions

In the second study case, detailed geometry of used small drop tube furnace (DTF) is shown in **Figure 10**. DTF can generate results in efficient time and cost, with similar results to those

http://dx.doi.org/10.5772/intechopen.70561

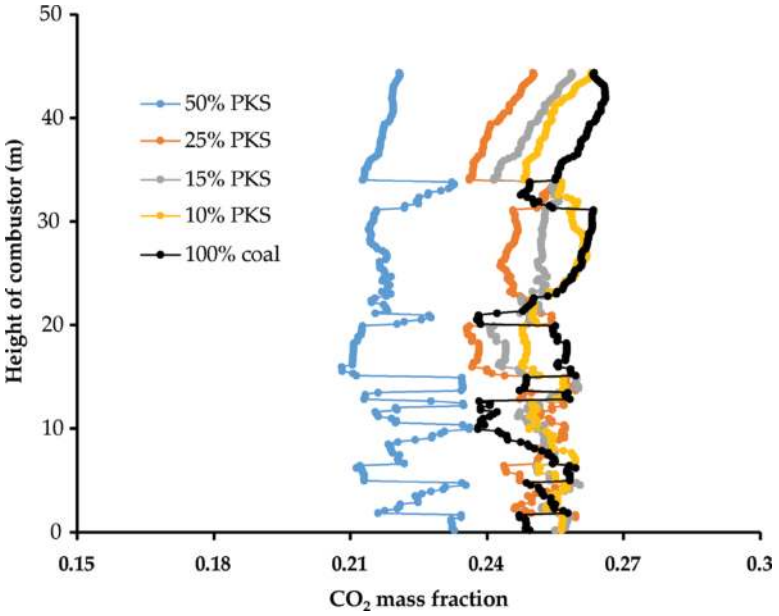

Figure 5. CO_2 distribution at the center along the height of the boiler at each different PKS mass fraction.

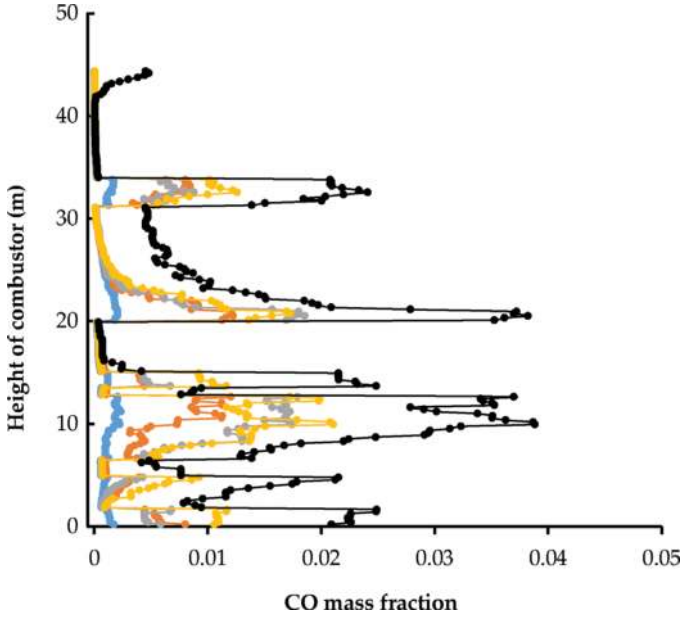

Figure 6. CO distribution at the center along the height of the boiler at each different PKS mass fraction.

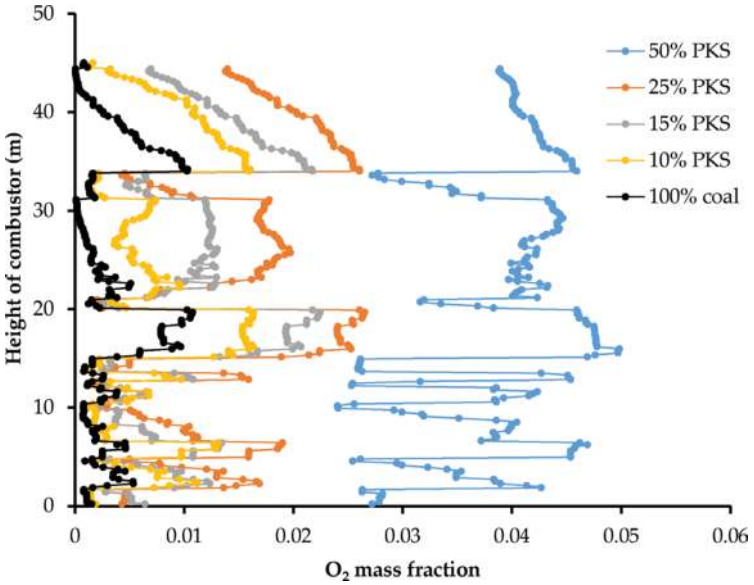

Figure 7. O_2 distribution at the center along the height of the boiler at each different PKS mass fraction.

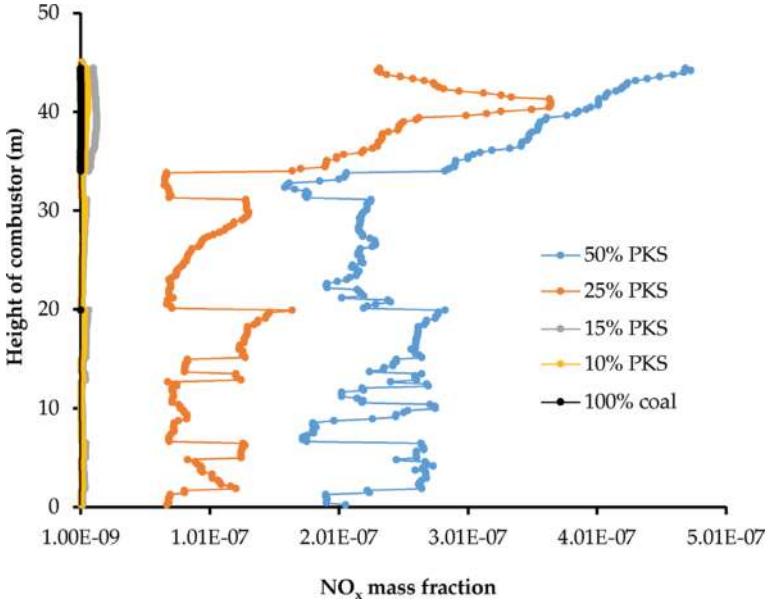

Figure 8. NO_x distribution at the center along the height of the boiler at each different PKS mass fraction.

http://dx.doi.org/10.5772/intechopen.70561

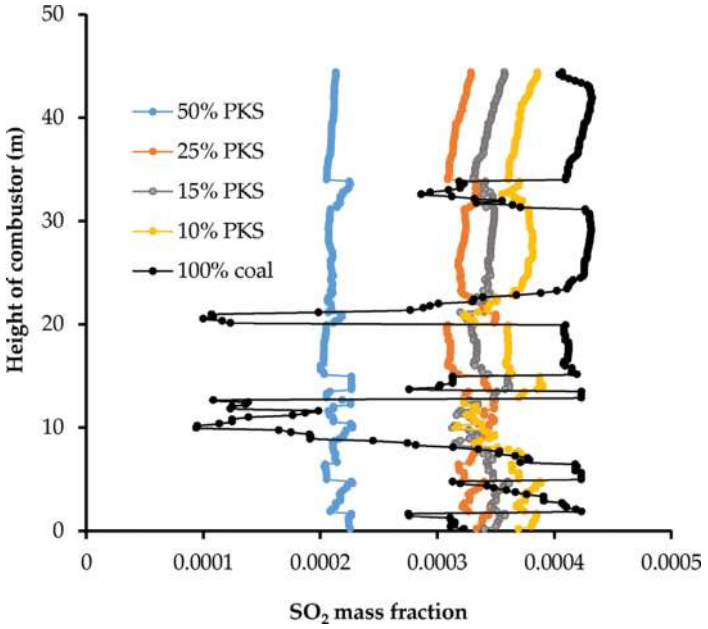

Figure 9. SO_2 distribution at the center along the height of the boiler at each different PKS mass fraction.

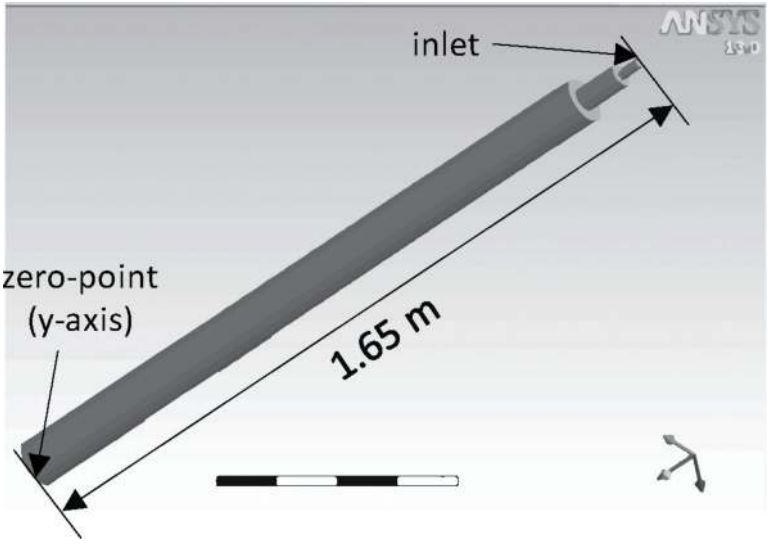

Figure 10. Geometry of DTF or combustor used in the simulation [2].

conducted in the real boiler. The combustion process takes place inside the tubular furnace and in the downward direction. The detailed report of this study can be read in the full paper written by Darmawan et al. [2].

The coal used in the simulation is originated from Kalimantan, Indonesia. This coal is classified as low rank coal having high moisture content and lower calorific value. On the other hand, the biomass, which is EFB, is hydrothermally treated in order to reduce the moisture content, increase the calorific value, and improve the mechanical properties [20, 21]. Hydrothermal treatment (HT) is also generally known as wet torrefaction [22]. **Table 2** shows the compositions of used coal and HT-EFB including proximate and ultimate analyses.

In the simulation, a commercial CFD software ANSYS DesignModeler and Fluent ver. 16.2 (ANSYS Inc.) are used to build 3D combustor model and analyze the cofiring behavior. As discussed earlier, cofiring simulation includes some considerations of dynamics equations, conservation of mass (continuity), momentum and enthalpy, turbulence (k-ε turbulence model), radiation heat transfer (P-1 model), and reactions in both particles (Eulerian-Lagrangian model) and gas (global two-steps reactions) phases. Some additional boundary conditions include (1) fuel and air inlet flow rates that are 1.38×10^{-5} kg s^{-1} and 1.6×10^{-4} kg s^{-1} at 300 K, (2) furnace wall temperature, wall roughness, and internal emissivity that are set to 1300 K (isothermal), 0.5, and 1, respectively, and (3) feeding wall is considered isothermal at 300 K.

4.2.2. Results and discussion

An HT-EFB after hydrothermal treatment is found to become more uniform and coal-like. Hydrothermal treatment also can improve the drying and dehydration performance, thus the moisture content of the HT-EFB decreases to approximately 3%. This characteristic is very important in the combustion system. **Figures 10** and **11** [3] show the temperature distribution along the axis of the DTF under different cofiring mass fractions. The figure excludes axis of the DTF at high temperatures of 0–0.6 m considering that there is no substantial change in the bottom of DTF and can be neglected. The dots in **Figure 11** correspond to the measured result

Components	Raw coal [3]	Dried coal [3]	Raw EFB [23]	HT-EFB [24]
Proximate analysis				
Fixed carbon (wt% wb)	24.93	40.23	3.71	28.62
Volatile matter (wt% wb)	25.76	41.57	34.84	62.57
Moisture (wt% wb)	48.76	17.30	60.00	3.00
Ash (wt% wb)	0.56	0.90	1.46	5.82
Ultimate analysis				
C (wt% wb)	35.30	56.98	17.97	52.92
H (wt% wb)	2.29	3.69	2.49	5.35
O (wt% wb)	11.23	18.13	17.60	32.06
N (wt% wb)	1.75	2.83	0.47	0.85
S (wt% wb)	0.11	0.17	0.01	0.00
Calorific value (MJ kg^{-1})	13.84	22.34	17.02	22.22

Table 2. Material composition.

http://dx.doi.org/10.5772/intechopen.70561

obtained from experimental validation for coal. In general, higher HT-EFB mass fraction will increase the temperature inside the combustor. HT-EFB mass fractions of 50% result in the highest outlet temperature (maximum of 1536 K) (**Figure 12**).

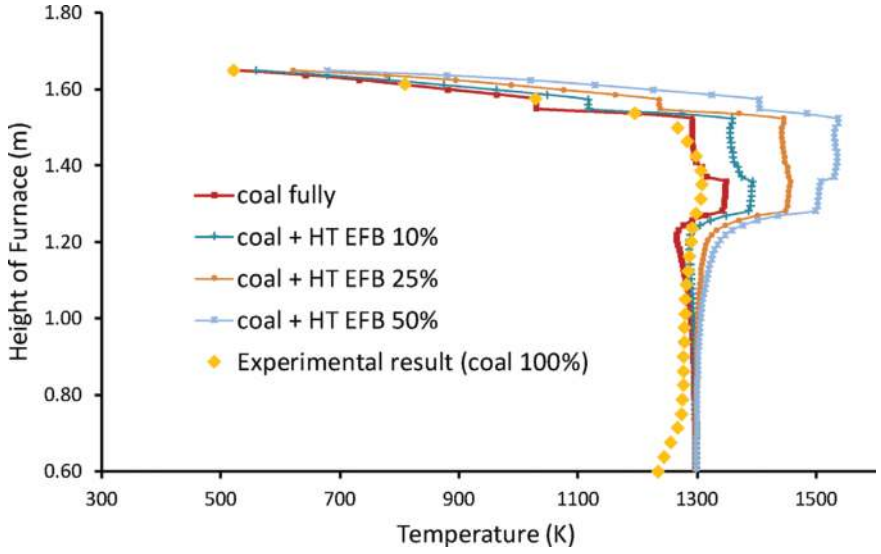

Figure 11. Temperature distribution inside the combustor of HT-EFB cofiring.

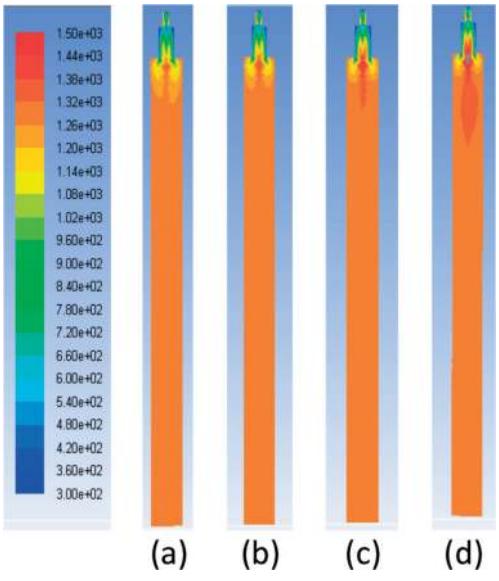

Figure 12. Temperature distribution of coal and HT-EFB cofiring across the combustor: (a) coal fully (b) HT-EFB 10% (c) HT-EFB 25% (d) HT-EFB 50%.

Fuel combustion process involves three basics stages as mentioned in Section 3: devolatilization, volatile combustion, and char oxidation. Compared to the main combustion area, a lower temperature is observed in the upper part of the combustor where the devolatilization process occurred. The mixture is pyrolyzed and then evolves as volatile matter. The devolatilization of HT-EFB particles occurs earlier and in a shorter time than coal because of lower moisture content of HT-EFB and higher volatile matter content. On the other hand, since coal has significantly higher moisture content, its particles require a longer time for drying and the devolatilization to occur. Therefore, in high HT-EFB mass fraction, the flame temperature remains high and distributed more uniformly although it is located in a lower part of the combustor. In addition, as HT-EFB has a lower moisture content than coal, high HT-EFB mass fraction leads to the lower total moisture content of the mixed fuel of HT-EFB and coal in the combustor system. Finally, this condition affects the flame temperature due to high heat capacity of water.

4.2.3. Distribution of produced CO and CO_2

In contrast to the fuel coal combustion, HT-EFB cofiring has increased carbon monoxide concentrations and nitrogen monoxide in the combustion. **Figures 13** and **14** [3] represent further information about the concentration of CO and CO_2 gases during cofiring.

Regarding the produced CO concentration, higher mass fraction of HT-EFB leads to the increase of CO mass fraction during initial reaction of combustion. The volatile matter, especially from

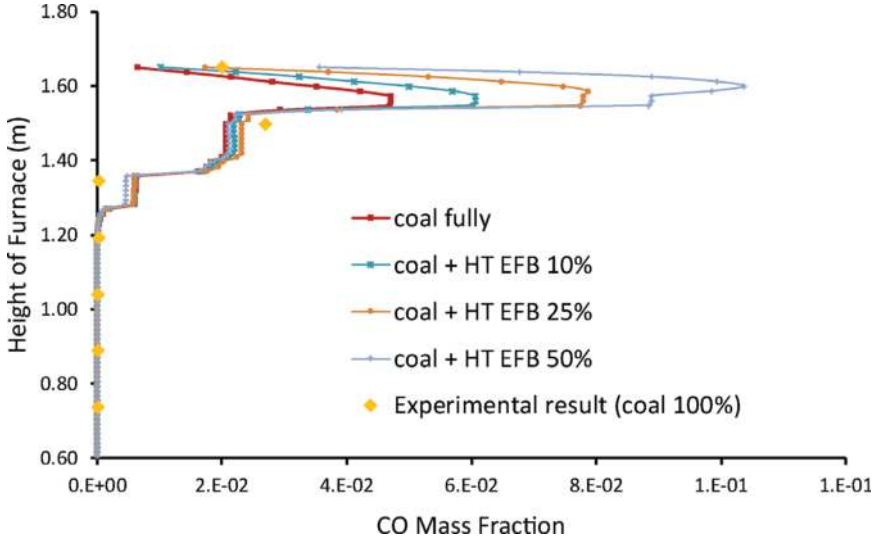

Figure 13. CO mass fraction along the combustor height under different HT-EFB mass fractions.

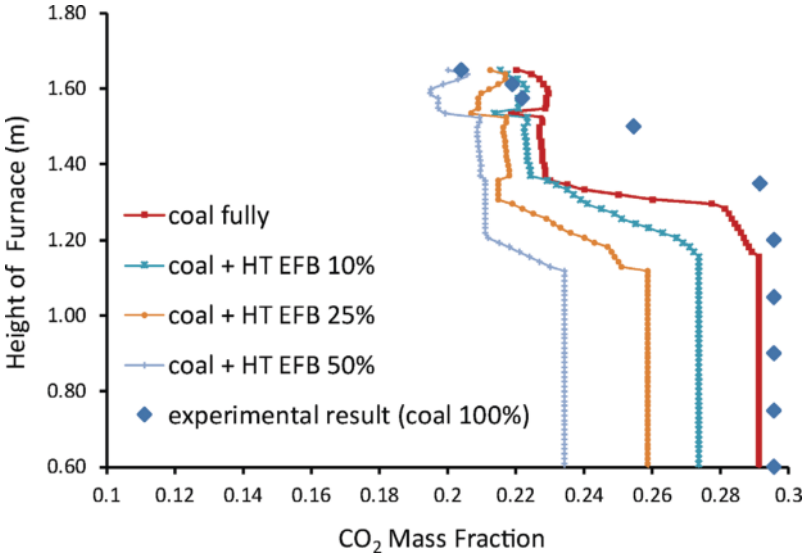

Figure 14. CO_2 mass fraction along the combustor height under different HT-EFB mass fraction.

HT-EFB, is oxidized under high combustion temperature forming CO. Afterward, CO reacts further with O_2 (air) along the combustor forming CO_2. In addition, coal cofiring with HT-EFB results in lower CO_2 concentration following the increase of both HT-EFB mass fraction (**Figure 9**). The dots in **Figure 10** show the CO_2 pollutant observed during the experimental study; meanwhile, the lines show CO_2 emission based on a simulation model.

5. Conclusion

Cofiring of biomass waste in a pulverized coal power plant was studied using CFD. This chapter has discussed performance for all stages of the combustion including the combustion temperatures, kinetics behavior, and concentration of the produced gases (CO_2, CO, O_2, NO_x, and SO_x). Moreover, the current state-of-the-art CFD modeling-based study is capable of solving the complexity of the interdependent processes such as turbulence, heat transfer via radiation, complex reactions in both the particle, and gas phases and the produced gas.

For further development, cofiring of biomass waste with coal can be clarified by a pilot experimental scale before being applied in full-scale power plants. This validation is necessary after conducting CFD simulation. To be remembered, it is also very important to take account of the biomass waste supply from the surrounding resources to avoid potential conflict with food production or prevent from potential shortage of sustainable biomass supply.

Acknowledgements

This work was partially supported by Indonesian government, which contributed to it through the program of the Indonesia Endowment Fund for Education (LPDP).

Author details

Arif Darmawan[1,2], Dwika Budianto[2], Koji Tokimatsu[1] and Muhammad Aziz[3]*

*Address all correspondence to: aziz.m.aa@m.titech.ac.jp

1 Department of Transdisciplinary Science and Engineering, Tokyo Institute of Technology, Yokohama, Kanagawa, Japan

2 Agency for the Assessment and Application of Technology, Serpong, Tangerang Selatan, Indonesia

3 Institute of Innovative Research, Tokyo Institute of Technology, Meguro, Tokyo, Japan

References

[1] Livingston WR Biomass ash and the mixed ashes from cofiring biomass with coal. In: Proceedings of the IEA Clean Coal Workshop, 25–26 January 2011, Drax Power Station, London, UK

[2] Darmawan A, Dwika D, Aziz M, Tokimatsu T. Retrofitting existing coal power plants through cofiring with hydrothermally treated empty fruit bunch and a novel integrated system. Applied Energy. 2017;**204**:1138-1147

[3] Aziz M, Dwika B, Oda T. Computational fluid dynamic analysis of cofiring of palm kernel shell into coal fired power plant. Energies. 2016;**9**:137. DOI: 10.3390/en9030137

[4] Xu W, Niu Y, Tan H, Wang D, Du W, Hui S. A new agro/forestry residues cofiring model in a large pulverized coal furnace: Technical and economic assessments. Energies. 2013;**6**:4377-4393

[5] IEA. Energy Technology Perspectives: Scenarios & Strategies to 2050. Paris: OECD/IEA; 2010

[6] IEA. World Energy Outlook 2010. Paris: OECD/IEA; 2010

[7] Williams A, Pourkashanian M, Jones JM. The combustion of coal and some other solid fuels. Symposium (International) on Combustion. 2000;**28**(2):2141-2162

[8] Tabet F, Gokalp I. Review on CFD based models for cofiring coal and biomass. Renewable and Sustainable Energy Reviews. 2015;**51**:1101-1114

[9] Ranade VV, Gupta DF. Computational Modeling of Pulverized Coal Fired Boilers. Boca Raton, USA: CRC Press; 2015

[10] Budianto D, Aziz M, Cahyadi, Oda T. Numerical investigation of cofiring of palm kernel shell into pulverized coal combustion. Journal of the Japan Institute of Energy. 2016;**95**: 605-614

[11] Oevermann M, Gerber S, Behrendt F. Euler-Lagrange/DEM simulation of wood gasification in a bubbling fluidized bed reactor. Particuology. 2009;**7**:307-316

[12] Anderson JD. Governing equations of fluid dynamics. In: Wendt JF, editor. Computational Fluid Dynamics. Berlin, Germany: Springer-Verlag; 2009. p. 15–51.

[13] Hu Z, Ma X, Chen Y, Liao Y, Wua J, Yu Z, et al. Co-combustion of coal with printing and dyeing sludge: Numerical simulation of the process and related NO_X emissions. Fuel. 2015;**139**:606-613

[14] Eaton AM, Smoot LD, Hill SC, Eatough CN. Components, formulations, solutions, evaluation, and application of comprehensive combustion models. Progress in Energy and Combustion Science. 1999;**25**:387-436

[15] Aziz M, Oda T, Kashiwagi T. Design and analysis of energy-efficient integrated crude palm oil and palm kernel oil processes. Journal of the Japan Institute of Energy. 2014;**94**:143-150

[16] Aziz M, Kurniawan T, Oda T, Kashiwagi T. Advanced power generation using biomass wastes from palm oil mills. Applied Thermal Engineering. 2017;**114**:1378-1386

[17] Aziz M, Prawisudha P, Prabowo B, Budiman BA. Integration of energy-efficient empty fruit bunch drying with gasification/combined cycle systems. Applied Energy. 2015;**139**: 188-195

[18] Aziz M, Kurniawan T. Enhanced utilization of palm oil mill wastes for power generation. Chemical Engineering Transactions. 2016;**52**:727-732

[19] Clean Air Technology Center (MD-12), Nitrogen Oxides (NOx), Why and How they are Controlled, Technical Bulletin of Environmental Protection Agency, EPA 456/F-99-006R, 1999, North Carolina, USA. Available from: http://www3.epa.gov/ttncatc1/cica/other7_e.html (accessed on Dec 2015)

[20] Zaini IN, Novianti S, Nurdiawati A, Irhamna AR, Aziz M, Yoshikawa K. Investigation of the physical characteristics of washed hydrochar pellets made from empty fruit bunch. Fuel Processing Technology. 2017;**160**:109-120

[21] Lokahita B, Aziz M, Yoshikawa K, Takahashi F. Energy and resource recovery from tetra Pak waste using hydrothermal treatment. Applied Energy. in press. DOI: 10.1016/j.apenergy.2017.05.141

[22] Mu'min GF, Prawisudha P, Zaini IN, Aziz M, Pasek AD. Municipal solid waste processing and separation employing wet torrefaction for alternative fuel production and aluminum reclamation.Waste Management. 2017;**67**:106-120

[23] Lam PS, Lam PY, Sokhansanj S, Lim CJ, Bi XT, Stephen JD, Pribowo A, Mabee WE. Steam explosion of oil palm residues for the production of durable pellets. Applied Energy. 2015;**141**:160-166

[24] Novianti S, Biddinika MK, Prawisudha P, Yoshikawa K. Upgrading of palm oil empty fruit bunch employing hydrothermal treatment in lab-scale and pilot scale. Procedia Environmental Sciences. 2014;**20**:46-54